AIP | Applied Physics Letters

Single-mode surface-emitting concentric-circular-grating terahertz quantum cascade lasers

Guozhen Liang, Houkun Liang, Ying Zhang, Suraj P. Khanna, Lianhe Li et al.

Citation: Appl. Phys. Lett. **102**, 031119 (2013); doi: 10.1063/1.4789535
View online: http://dx.doi.org/10.1063/1.4789535
View Table of Contents: http://apl.aip.org/resource/1/APPLAB/v102/i3
Published by the AIP Publishing LLC.

Single-mode surface-emitting concentric-circular-grating terahertz quantum cascade lasers

Guozhen Liang,[1] Houkun Liang,[2] Ying Zhang,[2] Suraj P. Khanna,[3] Lianhe Li,[3] A. Giles Davies,[3] Edmund Linfield,[3] Dau Fatt Lim,[1] Chuan Seng Tan,[1] Siu Fung Yu,[4] Hui Chun Liu,[5] and Qi Jie Wang[1,6,a)]

[1]*School of Electrical and Electronic Engineering, Nanyang Technological University, 50 Nanyang Avenue, 639798 Singapore*
[2]*Singapore Institute of Manufacturing Technology, 71 Nanyang Drive, 638075 Singapore*
[3]*School of Electronic and Electrical Engineering, University of Leeds, Leeds LS2 9JT, United Kingdom*
[4]*Department of Applied Physics, Hong Kong Polytechnic University, Kowloon, Hong Kong*
[5]*Key Laboratory of Artificial Structures and Quantum Control, Department of Physics, Shanghai Jiao Tong University, Shanghai 200240, China*
[6]*School of Physical and Mathematical Sciences, Nanyang Technological University, 50 Nanyang Avenue, 637371 Singapore*

(Received 19 November 2012; accepted 11 January 2013; published online 25 January 2013)

We demonstrate single-mode surface-emitting terahertz frequency quantum cascade lasers utilising non-uniform second-order distributed feedback concentric-circular-gratings. The grating is designed for single-mode operation and surface emission for efficient and directional optical power out-coupling. The devices exhibit single-mode operation over the entire dynamic range with a side-mode-suppression-ratio of around 30 dB at 78 K, and a six-fold rotationally symmetric far-field pattern. In addition, the devices show a peak output power approximately three times higher than in ridge-waveguide lasers of similar size, whilst maintaining similar threshold current densities for the 3.8 THz emission and without remarkably sacrificing the maximum temperature operation performance. Owing to the high symmetry of the structure and the broad area light emission from surface, the devices are potentially very suitable for use as single-mode, high power emitters for integration into two-dimensional laser arrays. © *2013 American Institute of Physics*.
[http://dx.doi.org/10.1063/1.4789535]

Terahertz (THz) frequency quantum cascade lasers (QCLs) have emerged as a compact semiconductor source of coherent THz radiation since their first demonstration in 2002,[1,2] and have promise for exploitation in THz applications such as spectroscopy,[3] heterodyne detection,[4] and imaging.[5] For most of these applications, high power single-mode lasers accompanied by low beam divergence are highly desirable. However, owing to the lack of a mode-selection mechanism, and the sub-wavelength mode confinement inherent particularly to metal-metal waveguides, conventional edge-emitting ridge-waveguide THz QCLs suffer from multiple-mode operation and an extremely wide beam divergence (∼180°). Moreover, the strong mode confinement in the laser cavity leads to a large impedance mismatch between the modes inside and outside the cavity, resulting in a low output power.

To overcome these drawbacks, approaches that use linear second-order distributed feedback (DFB) gratings[6,7] have been developed to couple the optical power vertically out of the laser cavity (i.e., surface emitting) and achieve a high output power and a low beam divergence, as well as single-mode emission. The surface emitted beam profiles are then typically two-dimensional (2D) ellipses. Although a low beam divergence is obtained in the direction parallel to the ridge axis,[6] the beam divergence angle is still large in the direction perpendicular to the laser ridge. Therefore, to achieve a narrow 2D symmetric far-field profile, several studies have bent the linear gratings into a ring structure, leading to second-order DFB ring grating QCLs.[8–10] Meanwhile, other techniques to improve beam divergence of THz QCLs have also been developed, such as collimated Si lens,[11] integrated spoof surface plasmon structure,[12] two-dimensional photonic crystal,[13] phase-locked arrays,[14] third-order Bragg grating,[15] etc.

Another potential way to overcome the drawbacks of ridge-waveguide THz QCLs is to use concentric-circular-gratings (CCGs).[16–18] In this letter, we demonstrate single-mode surface emitting second-order CCG DFB THz QCLs. The devices exhibit a single-mode operation over the full range of injection currents where lasing is observed, with a high side-mode-suppression-ratio (SMSR) of ∼30 dB. In addition, a six-fold rotationally symmetric far-field profile is observed which corresponds to the third-order azimuthal mode in the laser cavity. Furthermore, the surface emitting CCG THz QCLs show a high output coupling power in comparison with the ridge-waveguide lasers of similar area.

The active region design of the THz QCLs used in this letter is a re-growth of that reported in Ref. 19 but with a slightly higher doping in the active region. This wafer was first Au-Au thermocompression bonded to an n+ GaAs receptor wafer, and then the original QCL substrate was removed by lapping and selective chemical etching. After that, the highly absorptive contact layer of the active region was removed by using a H_2SO_4:H_2O_2:H_2O (1:7:80) solution to avoid loss of the THz radiation coupled out through the open regions of the grating. Top metal gratings (Ti/Au

a)Electronic mail: qjwang@ntu.edu.sg.

15/200 nm) were then defined by standard optical lithography and lift-off processes, following which the active region was wet-etched to form a disk structure using a H_3PO_4:H_2O_2:H_2O (1:1:10) solution with a photoresist (AZ5214) as the mask. The substrate was thinned to 150 μm, and a Ti/Au (20/300 nm) employed for the bottom contact. The sample was then cleaved, mounted onto Cu submounts, wired, and finally mounted onto the cold finger of a cryostat for measurement.

Figure 1 shows optical microscope images of a typical fabricated device. The radial standing wave modes inside the disk can be expressed by a superimposition of non-periodic Bessel functions.[20] This is in contrast to traditional second-order DFB ridge-waveguide lasers where a linear second-order grating is adopted, because the standing wave modes in the ridge cavities are expressed as sinusoidal waves. Thus, we design the CCG to be a non-uniform grating targeted for single-mode emission at ~3.8 THz. The width of all the open slits is 2 μm, which is relatively narrow to guarantee uniform current injection over the whole disk area. The slits have a small mark-to-space duty cycle of ~10% to achieve a low out-coupling loss so that the threshold of the CCG lasers is comparable with that of ridge-waveguide lasers. The size of the boundary region (without metal coverage) and the diameter of the center ring are optimized through simulations to be 24.2 μm and 46.8 μm, respectively. The radius of the whole disk is 352 μm. The whole designed grating structure starting from the center of disk to the boundary is as follows: 23.4/**2**/20.1/**2**/18.7/**2**/18.9/**2**/20.1/**2**/19.4/**2**/20.1/**2**/20.1/**2**/20.1/**2**/20.1/**2**/19.9/**2**/20.1/**2**/20.1/**2**/20.5/**2**/16.9/**24.2** μm, where bold number indicates the open slits. A three-spoke bridge structure is employed to connect all the rings together for electrical pumping of the whole device.

Figure 2(a) shows the light-current-voltage (LIV) characteristics of a typical CCG THz QCL for different operating temperatures, using a room-temperature pyroelectric detector. The laser operates up to 104 K in pulsed mode, under a 200 ns pulse width and a 10 kHz repetition rate. The maximum operating temperature of a ridge laser (125 μm wide and 2 mm long) processed from the same QCL wafer is around 130 K, under the same operating conditions. Figure 2(b)

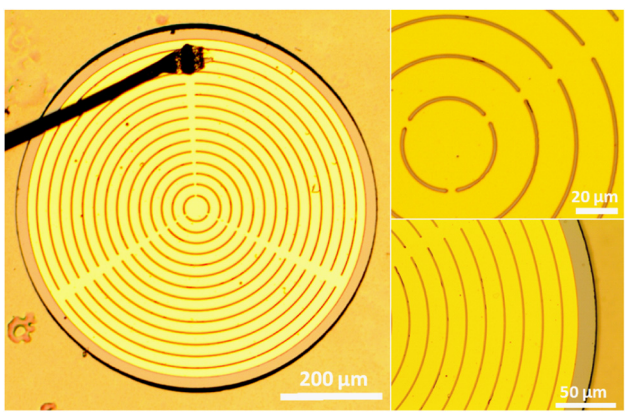

FIG. 1. Optical microscope images of a fabricated CCG DFB QCL. Left: A three-spoke bridge structure connects the metal gratings, allowing electrical pumping of the whole device. Right: Magnified images of the device showing the dimensions of the center ring and the boundary slit without metal coverage.

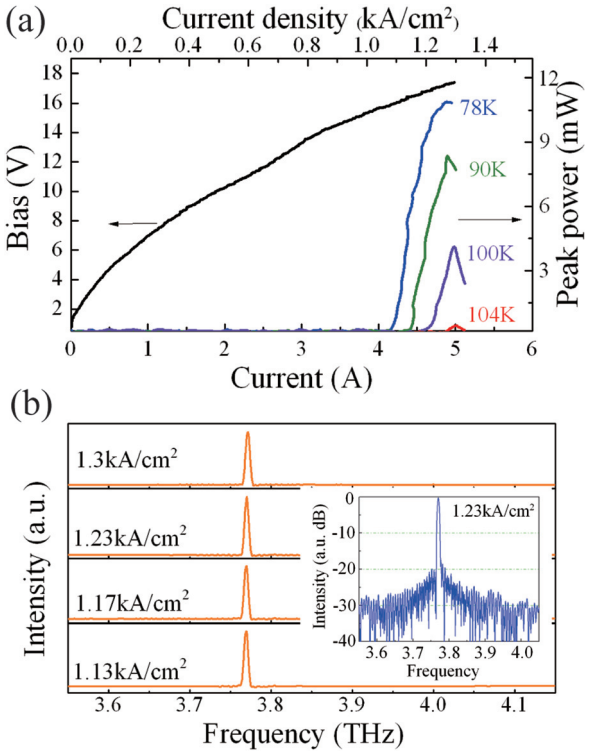

FIG. 2. Measured results of a CCG DFB laser. (a) Pulsed (200 ns pulses repeated at 10 kHz) LIV characteristics of the laser. (b) Emission spectra of the laser at 78 K for different injected current densities, from the threshold to the rollover. The inset shows a logarithmic scale plot of the spectrum, indicating a side-mode suppression ratio of around 30 dB.

shows the spectra of the CCG DFB THz QCL for different injected current densities at 78 K, from the threshold to the rollover. The device has a single-mode emission at ~3.8 THz for all drive currents. Limited by the noise level of the detector, a SMSR of around 30 dB can be measured at 78 K, as shown in the inset of Fig. 2(b), reflecting the strong single mode selectivity of the grating. Similar spectra were observed in several devices of the same grating design.

Figure 3 shows the LI curve of a CCG DFB QCL compared with that of a ridge-waveguide laser of similar area. An increased output power, by a factor of approximately three times, is measured. Owing to the Stark effect of the diagonal lasing transition, the emission frequency of the ridge-waveguide THz QCL shifts from 3.2 THz to 3.9 THz as the drive current increases, as shown in the inset of Figure 3. The CCG grating is designed only to select the ~3.8 THz mode, which does not lie in the gain spectrum (centered at 3.2 THz) at low drive currents (<1.1 kA/cm^2), and so this prevents a direct comparison of threshold current densities of the ridge-waveguide and CCG THz QCL. However, from the red dashed-dotted line in Fig. 3 which shows the characteristics of a ridge-waveguide laser at ~3.8 THz, one can still conclude that the two lasers have similar threshold current densities and dynamic ranges for 3.8 THz laser emission.

The 2D far-field profile of a CCG DFB QCL was measured by scanning a parabolic mirror (1° per step) with a 5 mm aperture on a spherical surface 15 cm in front of the laser. The purpose of using the 5 mm aperture is to guarantee a high angular resolution in the measurement. The incident radiation passing through the aperture was reflected by the parabolic mirror into a liquid-helium-cooled bolometer. As

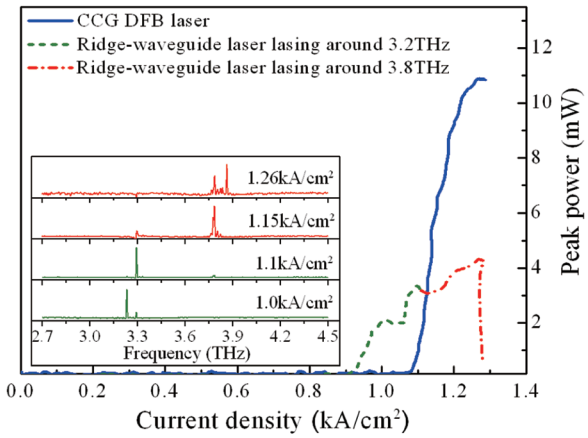

FIG. 3. Comparison of the LI characteristics of a CCG DFB QCL and a ridge-waveguide laser at 78 K. The CCG DFB laser operates only at 3.77 THz, whilst the ridge laser operates at ~3.2 THz (green portion of the LI curve) and ~3.8 THz (red portion of the LI curve) below and above a 1.1 kA/cm^2 current density, respectively. The inset shows the spectra of the ridge-waveguide laser under different drive currents.

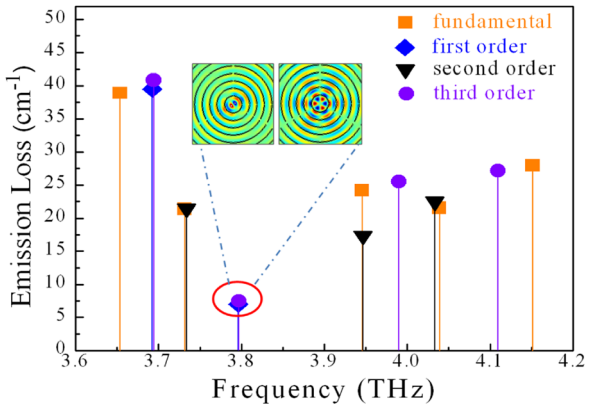

FIG. 5. Mode-spectrum of the CCG structure. Only the first four lowest order azimuthal modes are shown. One first-order and one third-order azimuthal modes have the lowest calculated losses at the lasing frequency, highlighted by the red circle. The mode distributions of the two modes are shown in the inset. Owing to the perturbation effects of the three-spoke bridge structure, only the third-order azimuthal mode achieved lasing in reality, as indicated by the far-field measurement represented in Fig. 4.

shown in Figure 4, the far-field pattern shows a six-fold rotational symmetry measured at 1.23 kA/cm^2, indicating that the lasing mode coupled from the CCG cavity is the third-order azimuthal mode, but not the fundamental azimuthal mode whose far-field pattern is a small ring. Using 2D numerical simulations (Comsol Multiphysics), and an approximate method described in Ref. 21, the simulated far-field pattern is shown in Fig. 4(b), which well reproduces the main features of the measured far-field pattern.

To further investigate the mode characteristics of CCG DFB QCLs, the mode spectrum is plotted in Fig. 5, based on a 2D simulation of the top-view of the cavity, adding in losses in the open slit regions to take into account the surface emission loss (surface out coupling). Only the first four azimuthal modes are shown; the higher-order modes with higher losses are not plotted. Two modes appear with almost the same eigen-frequencies and losses (highlighted by a red circle) around the lasing frequency (~3.8 THz). One is the third-order azimuthal mode, whilst the other is the first-order azimuthal mode (Inset; Fig. 5). However, from the far-field measurements shown in Fig. 4, only the third-order azimuthal mode appears in the experimental results (the far-field pattern of the first-order azimuthal mode should be mainly a single spot located at (0, 0) in Fig. 4). We attribute this to the perturbation effects of the three-spoke bridge structure, which result in a lower loss for the third order azimuthal mode (the first order azimuthal mode has a higher overlap with the metal bridge structure (see the inset of Fig. 5), which induces higher losses due to the scattering effects. It is noted that the metal bridge structures function as more disturbing the light than guiding it because only a small portion of the mode is covered under the bridges.

It is worth mentioning that the device could also support whispering-gallery-like (WGL) modes, similar to those shown in Fig. 6(c), since the device has a disk structure. However, these WGL modes are suppressed by the unpumped and, thus, absorptive boundary. Moreover, even if those WGL modes are excited, they will be well confined in the cavity with very low out-coupling efficiencies, preventing

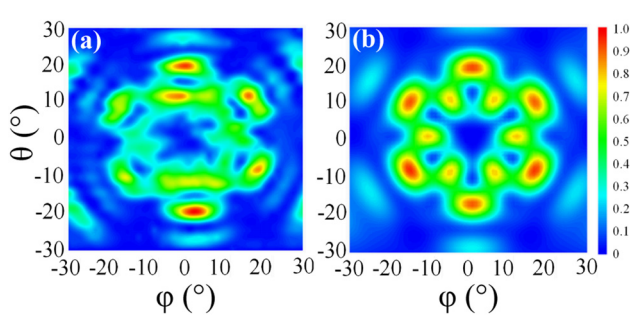

FIG. 4. Two-dimensional far-field emission patterns of the CCG DFB QCL. (a) The experimentally measured emission, and (b) the simulated emission of the third-order azimuthal mode.

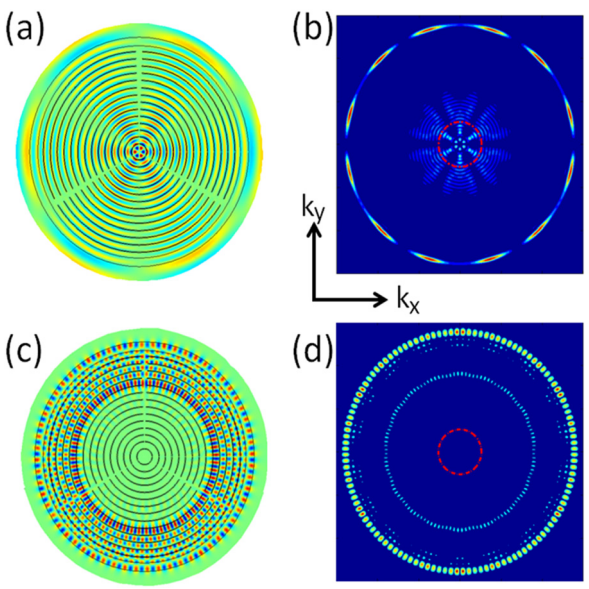

FIG. 6. Supported modes in the CCG DFB QCLs, and the corresponding momentum space intensity distributions. (a) Electric field intensity of the third-order azimuthal lasing mode and (c) a WGL mode. (b) and (d) are in-plane momentum-space intensity distributions for the modes in (a) and (c), respectively. The red dashed circle represents the light-cone—only radiation components inside the light-cone can be out-coupled. There are no intensity components in the light-cone for the WGL mode, in contrast to the situation for the third-order CCG mode.

them from being observed experimentally in the far-field. To gain insight into the behavior of these WGL modes, we calculated the momentum-space intensity distributions by using the Fourier transform of the in-plane fields (Figs. 6(b) and 6(d)).[22] The red dashed circle in each figure represents the light-cone defined as $k_x^2 + k_y^2 = (\omega/c)^2$, where only the radiation components inside the light-cone can be out-coupled. As there is no observable component in the light-cone (Fig. 6(d)) for the WGL modes, such modes cannot contribute to the far-field radiation. This contrasts with CCG modes, where efficient out-coupling can be expected.

In conclusion, we have demonstrated single-mode surface emitting THz QCLs using second-order CCGs, which can be simply fabricated by metal evaporation on top of the laser active region. We have achieved a side-mode suppression ratio of around 30 dB at 78 K with a concentrated six-fold rotationally symmetric far-field pattern, which corresponds to the third-order azimuthal mode. We show that the CCG DFB QCL has a similar threshold current to a ridge laser of comparable area, but with a three-fold increase in output power. Furthermore, compared with ring grating DFB QCLs, the emission of the CCG DFB QCLs can be designed to be evenly distributed across the top surface, potentially leading to a further improved beam divergence.

This work is supported by A*STAR SERC Singapore under Grant No. 082-101-0016; Nanyang Technological University under Grant No. M58040017; and the Tier 2 Grant funded by Ministry of Education, Singapore (MOE2011-T2-2-147). A.G.D. and E.H.L. acknowledge support of the EPSRC (UK), the EC programmes *NOTES* and *TOSCA*, the Royal Society, and the Wolfson Foundation. H.C.L. thanks supports from the National Major Basic Research Projects (2011CB925603) and the Shanghai Municipal Major Basic Research Project (09DJ1400102).

[1]R. Köhler, A. Tredicucci, F. Beltram, H. E. Beere, E. H. Linfield, A. G. Davies, D. A. Ritchie, R. C. Iotti, and F. Rossi, Nature **417**, 156–159 (2002).
[2]B. S. Williams, Nature Photon. **1**, 517–525 (2007).
[3]H.-W. Hubers, S. G. Pavlov, H. Richter, A. D. Semenov, L. Mahler, A. Tredicucci, H. E. Beere, and D. A. Ritchie, Appl. Phys. Lett. **89**, 061115 (2006).
[4]J. R. Gao, J. N. Hovenier, Z. Q. Yang, J. J. A. Baselmans, A. Baryshev, M. Hajenius, T. M. Klapwijk, A. J. L. Adam, T. O. Klaassen, B. S. Williams, S. Kumar, Q. Hu, and J. L. Reno, Appl. Phys. Lett. **86**, 244104 (2005).
[5]K. L. Nguyen, M. L. Johns, L. Gladden, C. H. Worrall, P. Alexander, H. E. Beere, M. Pepper, D. A. Ritchie, J. Alton, S. Barbieri, and E. H. Linfield, Opt. Express **14**, 2123–2129 (2006).
[6]S. Kumar, B. S. Williams, Q. Qin, A. W. Lee, Q. Hu, and J. L. Reno, Opt. Express **15**, 113 (2007).
[7]J. A. Fan, M. A. Belkin, F. Capasso, S. Khanna, M. Lachab, A. G. Davies, and E. H. Linfield, Opt. Express **14**, 11672–11680 (2006).
[8]L. Mahler, M. I. Amanti, C. Walther, A. Tredicucci, F. Beltram, J. Faist, H. E. Beere, and D. A. Ritchie, Opt. Express **17**, 13031–13039 (2009).
[9]E. Mujagić, C. Deutsch, H. Detz, P. Klang, M. Nobile, A. M. Andrews, W. Schrenk, K. Unterrainer, and G. Strasser, Appl. Phys. Lett. **95**, 011120 (2009).
[10]L. Mahler, A. Tredicucci, F. Beltram, C. Walther, J. Faist, B. Witzigmann, H. E. Beere, and D. A. Ritchie, Nature Photon. **3**, 46–49 (2008).
[11]A. Wei Min Lee, Q. Qin, S. Kumar, B. S. Williams, Q. Hu, and J. L. Reno, Opt. Lett. **32**, 2840–2842 (2007).
[12]N. Yu, Q. J. Wang, M. A. Kats, J. A. Fan, S. P. Khanna, L. Li, A. G. Davies, E. H. Linfield, and F. Capasso, Nature Mater. **9**, 730–735 (2010).
[13]Y. Chassagneux, R. Colombelli, W. Maineult, S. Barbieri, H. E. Beere, D. A. Ritchie, S. P. Khanna, E. H. Linfield, and A. G. Davies, Nature **457**, 174–178 (2009).
[14]T.-Y. Kao, Q. Hu, and J. L. Reno, Appl. Phys. Lett. **96**, 101106 (2010).
[15]M. I. Amanti, M. Fischer, G. Scalari, M. Beck, and J. Faist, Nature Photon. **3**, 586–590 (2009).
[16]X. F. Li and S. F. Yu, J. Appl. Phys. **106**, 053103 (2009).
[17]R. H. Jordan, D. G. Hall, O. King, G. Wicks, and S. Rishton, J. Opt. Soc. Am. B **14**, 449 (1997).
[18]C. Olson, P. L. Greene, G. W. Wicks, D. G. Hall, and S. Rishton, Appl. Phys. Lett. **72**, 1284 (1998).
[19]S. Kumar, Q. Hu, and J. L. Reno, Appl. Phys. Lett. **94**, 131105 (2009).
[20]M. Toda, IEEE J. Quantum Electron. **26**, 473–481 (1990).
[21]Y. Chassagneux, R. Colombelli, W. Maineults, S. Barbieri, S. P. Khanna, E. H. Linfield, and A. G. Davies, Opt. Express **17**, 9491–9502 (2009).
[22]S.-H. Kim, S.-K. Kim, and Y.-H. Lee, Phys. Rev. B **73**, 235117 (2006).